AL-Saedi, Safaa I.; Haider, Adawiya J.; Naje, Asama N.; Bassil, Nathalie

Article

Improvement of Li-ion batteries energy storage by graphene additive

Energy Reports

Provided in Cooperation with:
Elsevier

Suggested Citation: AL-Saedi, Safaa I.; Haider, Adawiya J.; Naje, Asama N.; Bassil, Nathalie (2020) : Improvement of Li-ion batteries energy storage by graphene additive, Energy Reports, ISSN 2352-4847, Elsevier, Amsterdam, Vol. 6, Iss. 3, pp. 55-63, https://doi.org/10.1016/j.egyr.2019.10.019

Available online at www.sciencedirect.com
ScienceDirect
Energy Reports 6 (2020) 64–71
www.elsevier.com/locate/egyr

TMREES, EURACA, 04 to 06 September 2019, Athens, Greece

Improvement of Li-ion batteries energy storage by graphene additive

Safaa I. AL-Saedi[a], Adawiya J. Haider[b,*], Asama N. Naje[a], Nathalie Bassil[c]

[a] *Department of Physics, College of Science, University of Baghdad, Iraq*
[b] *Department of Applied Science, University of Technology, Iraq*
[c] *Faculty of Sciences, Lebanese University, 90656 Jdeidet el Metn, Lebanon*

Received 20 September 2019; accepted 18 October 2019
Available online 25 October 2019

Abstract

In this work, the layered compound of $LiCo_{0.525}Ni_{0.475}O_2$, (LCNO) was prepared by self-propagating combustion reaction for the cathode of lithium-ion battery. We used self-propagating combustion reaction to prepare the compound of $LiCo_{0.525}Ni_{0.475}O_2$, (LCNO) as a cathode material of lithium-ion battery, then we added Graphene (G) to LCNO as additive to obtain LCNO/G (LCNOG). Graphene weight is (4 %) of the total weight of LCNO, in a typical preparation, 10 g of LCNO, 0.4 g from G and 200 ml of ethanol were stirred together at room temperature to reach full dryness. We used thermo-gravimetric analysis (TGA) to determine the optimum range of annealing temperatures of LCNO and LCNOG. The value found were (650, 750 and 850) °C for 12 h in air. Changes in the structural and morphological properties were also studied.

The structural properties of LCNO and LCNOG powder were studied by means of X-ray diffraction (XRD), Field Emission Scanning Electron Microscopy (FE-SEM), Energy Dispersive Spectrometry (EDS), Atomic Force Microscopy (AFM) and a Vibrating Sample Magnetometer (VSM). XRD analysis shows that all the powders are crystallized in the Space group R-3m, crystal system is trigonal (hexagonal axes) and present a random orientation and surface morphology of the LCNOG powder consists of Nano-crystalline grains with uniform coverage of the substrate surface with randomly oriented. XRD analysis showed that all the powders are crystallized in the Space group R-3m, crystal system is trigonal (hexagonal axes) and present a random orientation. Surface morphology of the LCNOG powder consists of Nano-crystalline grains with uniform coverage of the substrate surface with random orientation. Hysteresis behavior analysis proved that the powder possessed soft magnetic properties. Thermo-gravimetric analysis showed that the best annealing temperature and duration that leads to particles in the range several nm of the targeted composition are 750 °C for 12 h.

Peer-review under responsibility of the scientific committee of the TMREES, EURACA, 2019.

Keywords: Lithium-ion; Batteries; Graphene; Nanostructures

1. Introduction

Li-ion batteries (LIBs) are one of the most common electrochemical energy storage systems at present, which have been widely used in areas from portable electronics to electric vehicles [1,2]. The main objective of global

* Corresponding author.
E-mail address: adawiyajumaa96@gmail.com (A.J. Haider).

https://doi.org/10.1016/j.egyr.2019.10.019

Peer-review under responsibility of the scientific committee of the TMREES, EURACA, 2019.

energy sustainability aims at the interchange of all fossil fuels (oil, coal, natural gas) with renewable energy sources (geothermal, hydrogen, batteries, etc.) [3]. The physical and chemical properties of electrode materials are considered to be the main factors to the energy density and effectiveness of LIBs. In general, the concentration of electrons (or holes) in the semiconductors is small, so that the magnetic exchange interactions are super exchange interactions [3–5]. That is why it is an important tool to characterize the sample, by detecting impurity phases or local defects.

One of the probable solutions to lithium ion batteries problems is to improve electrode materials. Since graphene has many unique properties like large surface to mass ratio, good chemical stability, and has very high electrical conductivity it was used by researchers to improve energy storage devices [6]. therefore many studies were done with graphene to improve the performance of solar cells [7], fuel cells [8], supercapacitors [9], Li-air batteries [10] and Li-ion batteries (as an additive to electrode [11,12]). So it has normally been considered as an ideal target for forming composite materials used as electrodes in Li-ion batteries.

An allotrope of carbon, graphene is a 2-D sheet material, made completely out of carbon atoms. It is only one atom in thickness as shown in Fig. 1.

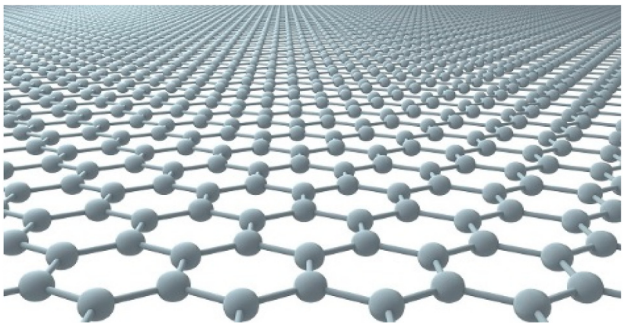

Fig. 1. Crystal structure of graphene compound [13].

It consists of sp2-hybridized carbon atoms organized in a honeycomb crystal lattice. It is a 2-dimensional structure, meaning that every atom of graphene can be considered as a surface atom [14]. Since graphene is made out of a single atomic layer of carbon, lithium ions can be put between two layers of graphene to make Li_2C_6, an excellent electrode material (with a specific capacity of 744 mAh g^{-1}) compared to traditional carbon anodes [15]

Graphene synthesize is done by two common methods: (the top-down and the bottom-up) method. In the top-down method, grapheme monolayers are obtained by separating the stacked graphite layers. To do so, one must break the van der waals forces joining the carbon layers [16]. However, there are some challenges with this method such as: defects of the surfaces of the graphene sheets and the discreteness of the sheets. That means that this approach offers low yield [16]. In the bottom-up approach, carbon molecules are used as building blocks [17]. However this approach is also not suitable to produce graphene sheets with a large surface area. The most common graphene production method was the mechanical cleavage of graphite. This method produces graphene with high-quality sheet and low defects [18]. Another effective method is chemical vapor deposition (CVD) [19,20]. All the above mechanism are low yield and require long time, but the mechanical cleavage methods help in the effective and full exploitation of these materials [21]. The graphite exfoliation is a suitable alternative method to synthesize graphene with high yield, low cost [22], furthermore it can be improved.

Improved Li-Ion electrodes allow for the storage of more lithium ions and increase the battery's capacity. Thus, the life of batteries containing graphene can essentially be longer than that of conventional batteries [23].

Energy is considered as one of the most important topic nowadays. Li-ion batteries (LIBs) are one of the most common rechargeable energy storage systems and are widely used in various fields such as (portable electronics, hybrid electrical vehicles, electrical cars etc.) [1]. The main theme of global energy supports is the exchange of all fossil fuels with renewable energy sources. Various cathode materials were presented like $LiCoO_2$ [24,25], $LiMn_2O_4$, and $LiFePO_4$ [26], however, their disadvantages like (high cost, toxicity and low operating voltage) [27], led the researchers to work seriously on improving and developing other alternative material for cathodes. In this paper we added Graphene (G) to $LiCo_{0.525}Ni_{0.475}O_2$, (LCNO) in order to improve the properties of cathode material.

2. Experimental work

$LiNO_3$, $Co(NO_3)_2 \cdot 6H_2O$, $Ni(NO_3)_2 \cdot 6H2O$ and $C_6H_6O_7$ of high purity (99.99%) were procured from Harris Chemicals Corporation in England. We used different weights set up as (6.8941 g of $LiNO_3$, 15.2740 g of $Co(NO_3)_2 \cdot 6H_2O$ and 13.808 g of $Ni(NO_3)_2 \cdot 6H_2O$. All nitrates were dissolved in deionized water and kept under magnetic stirring for 15 min at room temperature, then heated on hot-plate for 30 min [28–30] at 100 °C. Then the mixture was put in the furnace at 400 °C for 15 min to completely combust.

The combustion reaction is a chemical reaction affected by factors such as (the reactant materials and the rate of impurities in it). The combustion reaction takes place in two steps. During the first one the water evaporates and the mixture becomes more viscous [31,32]. The combustion starts when the water decreases to a critical point and the temperature raises to the threshold value. This corresponds to the amount of energy that must be provided to start the reaction. The second step begins when the reaction produces (hydroxide and nitric acid) due to the metals nitrates dissolved in water. Then intermediate compounds forms due to the addition of citric acid.

Thermal analysis of the powder sample was made using Thermo-gravimetric Analysis (TGA) STA-PT1000 from Lenses Germany. The factors of measurements were set up at (heating rate 10 °C/min with a constant atmospheric pressure). The use of TGA is to determine the optimum temperature at which impurities are removed as well as phase formation and crystallization.

X-ray diffraction (XRD-6000) using 2θ, operating at 40 kV and 30 mA, X-ray Cu Kα (1.540600 Å), was used to analyzed LCNOG mixture. Field Emission Scanning Electron Microscope (FE-SEM); MIRA3 TESCAN, helped investigating the topographies of the LCNOG mixture. Atomic Force Microscope (AFM) (Angstrom USA, Spm3000 system) was used to determine the particle size distribution. The magnetic properties were determined by a vibrating sample magnetometer VSM (Model VSMF 7407).

3. Results and discussion

Fig. 2. shows the TGA analysis curve that indicates a continuous decrease of mass with temperature. We considered three points on the plot for support analysis. The first point was set at 100 °C for which the mass loss was (4.98 mg) with an endothermic peak resulting from the evaporation of residual water in LCNOG mixture. At about 541 °C the second mass loss occurred that corresponded to an exothermic peak, when all the unreacted materials combusted. A pure phase of the material formed at the third point at 700 °C [26,28–33]. Lithium oxide is decomposed at annealing temperatures higher than 850 °C. A structurally bestead compound may be formed at these high temperatures when excluded long annealing hours.

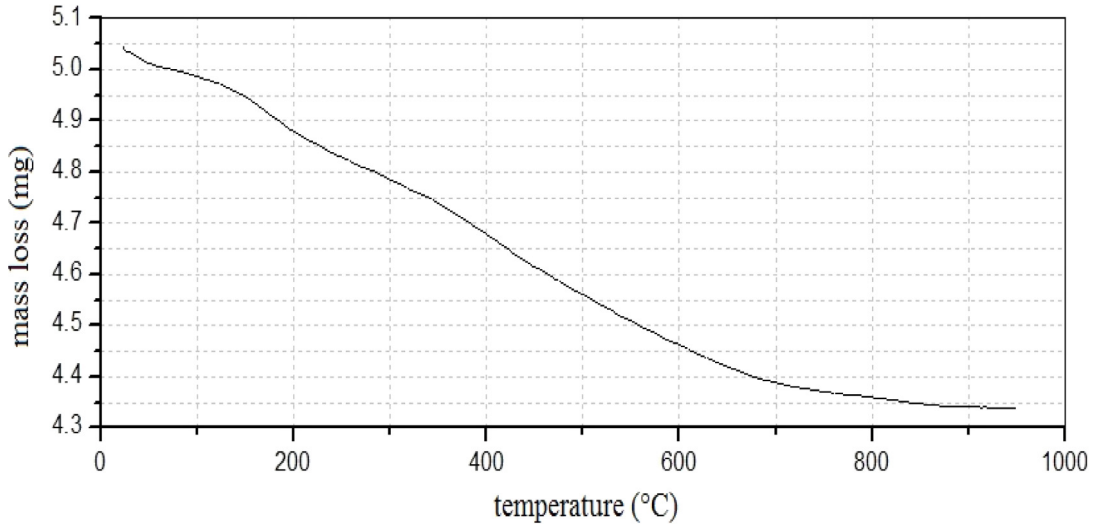

Fig. 2. Results of the TG for LCNOG material.

Depending on the TG analysis we chose (650, 750 and 850 °C) as annealing temperatures to treat LCNOG powders. Accordingly, powders were categorized P650, P750 and P850.

We used the X-ray energy dispersive spectroscopy (EDS) to detect the elements of the material as shown in Fig. 3. We found that the weight percentages of Co, Ni, O and C were 32.41, 26.86, 35.80 and 4.92 respectively. The results of EDS are in agreement with XRD results [29,34–36].

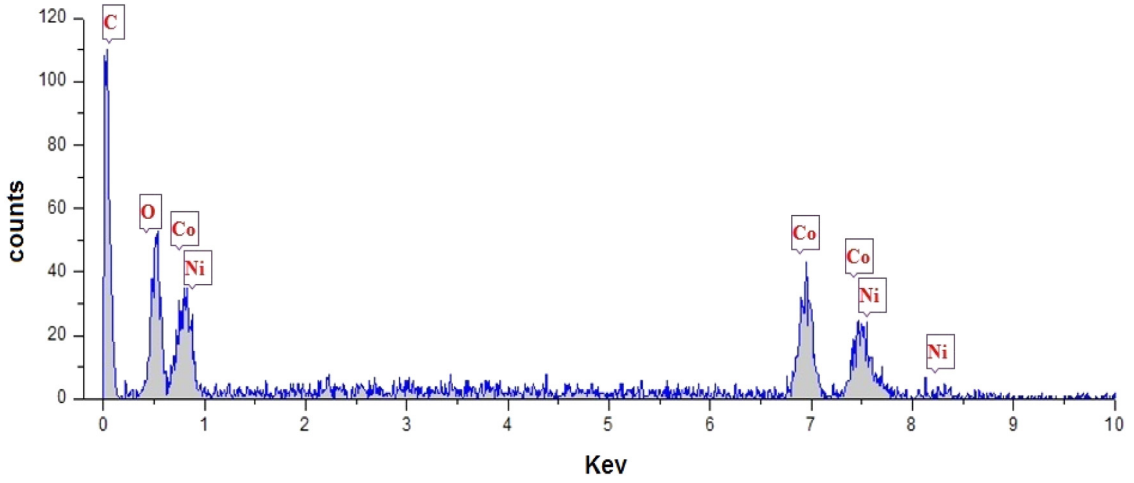

Fig. 3. Energy dispersive spectrum of $LiCo_{0.525}Ni_{0.475}O_2$/ graphene (LCNOG) cathode active material.

The X-ray diffraction spectra for pure and doped LCNOG before and after annealing are reported in Fig. 4. Generally, all the X-ray patterns showed high intensity peaks that indicate a good crystallinity in the annealed simples. Additionally, all samples exhibited similar peaks.

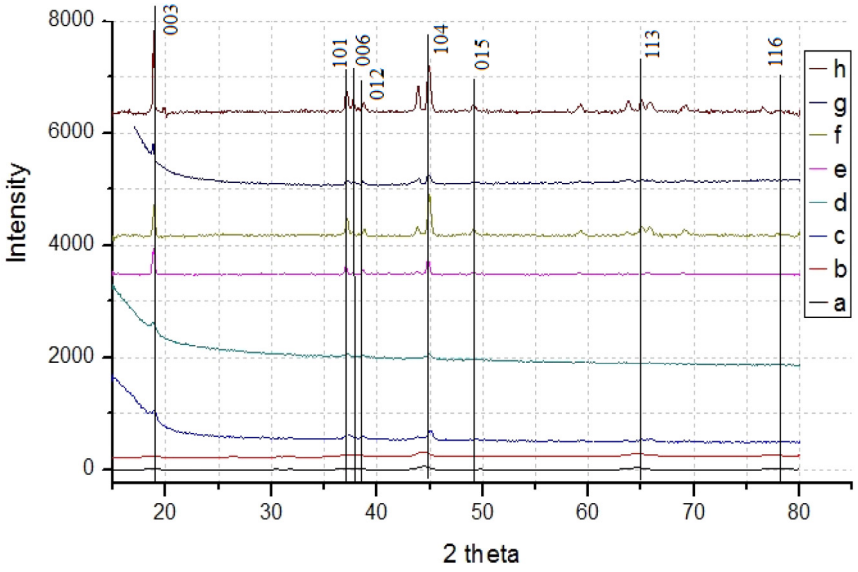

Fig. 4. XRD patterns of (a) LCNO before annealing (b) LCNOG before annealing (c) LCNO at 650 °C (d) LCNOG at 650 °C (e) LCNO at 750 °C (f) LCNOG at 750 °C (g) LCNO at 850 °C (h) LCNOG at 850 °C.

The diffraction patterns can be indexed with the $LiNiO_2$ pattern (ICDD no 98-003-4550). The materials have the hexagonal α- $NaFeO_2$ structure with R-3 m space group, which is also the same structure as $LiCoO_2$. The diffraction patterns indicated that all the materials are pure and single phase. No impurity peaks are observed. Before annealing, the peak of graphene was detected at $2\theta \sim 26.6°$ corresponding to a d-spacing of 0.335 nm which is close to the graphite d-spacing. After the annealing, the peak of graphene was not seen very clearly. This may be attributed to the low doping concentration of graphene and to the high peaks intensity of LCNO after annealing.

The X-ray spectra of LCNOG before and after annealing show main peaks which were located at about $2\theta =$ (18.841, 37.110, 38.129, 38.767, 44.823, 49.063, 65.781, and 78.647) and were attributed to LiCoO2 (003), (101),

LiNiO2 (006), LiNiO2 (012), (104), (015) and LiCoO2 (113) and (116), respectively, this agrees with the result obtained by Kalyani et al. 2005 [37].

By using SEM images we described the topographic and particle distribution in LCNOG as shown in Fig. 5a–c. It was observed that the size of the formed particles is between 5 and 150 nm. In addition, when the annealing temperature increases the particles aggregate and their sizes increases too as shown in Fig. 5.

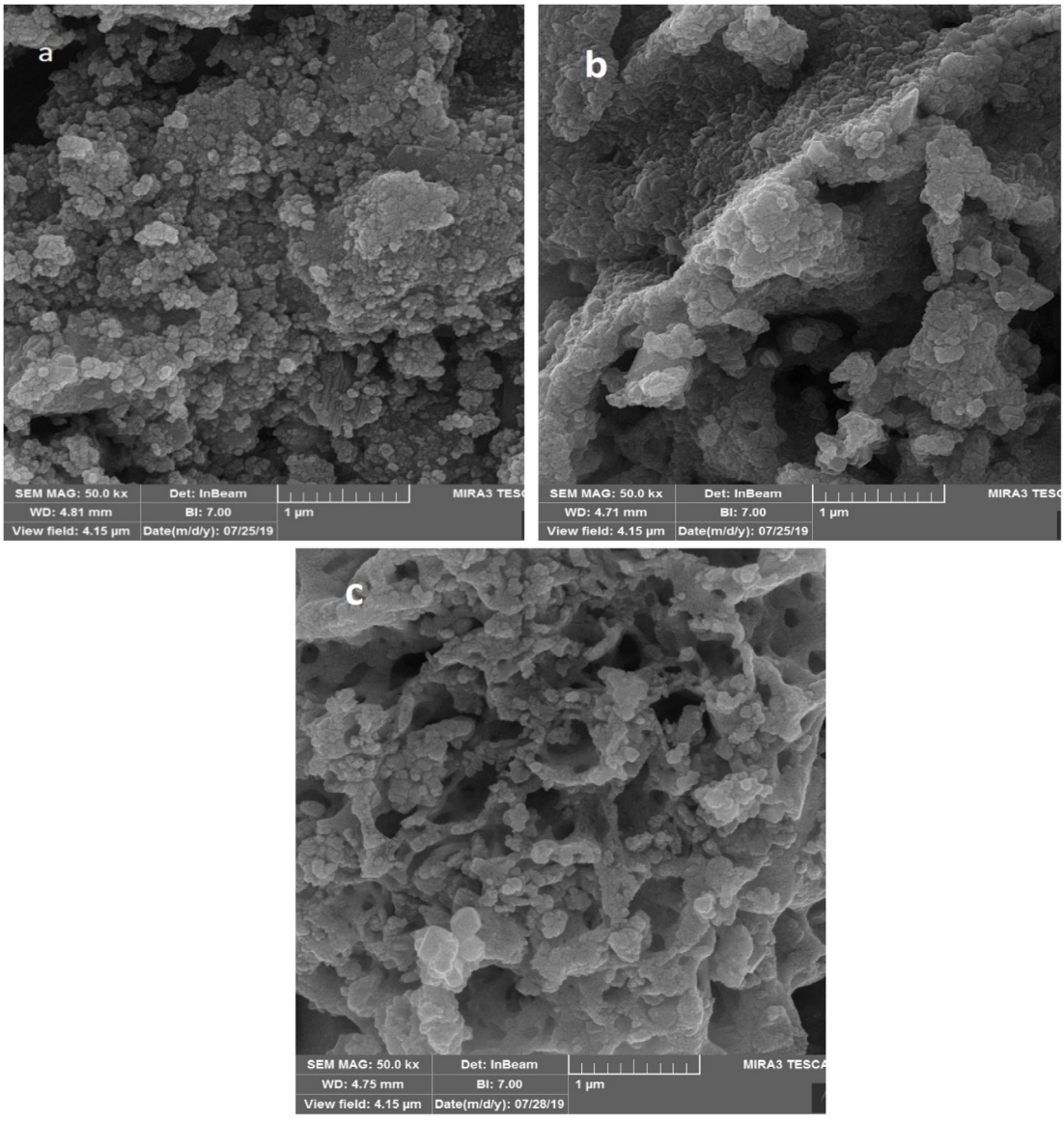

Fig. 5. FE-SEM images of LCNOG materials at different annealing temperature (a) 650 °C (b) 750 °C (c) 850 °C.

At high annealing temperature, the particle size increases while the distances between the particles become smaller and more regular as shown in Fig. 5. These results were in agreement with Ref. [36]. LCNOG may have promising electrochemical features, which can be improved by decreasing the diffusion and the distances between the particles.

By using Atomic Force Microscopy (AFM) as shown in Fig. 6 We obtained a 3D of the topographical structure of (LNCOG) for the samples with annealing temperature (650, 750 and 850) °C. The area scanned was about 3 μm × 3 μm.

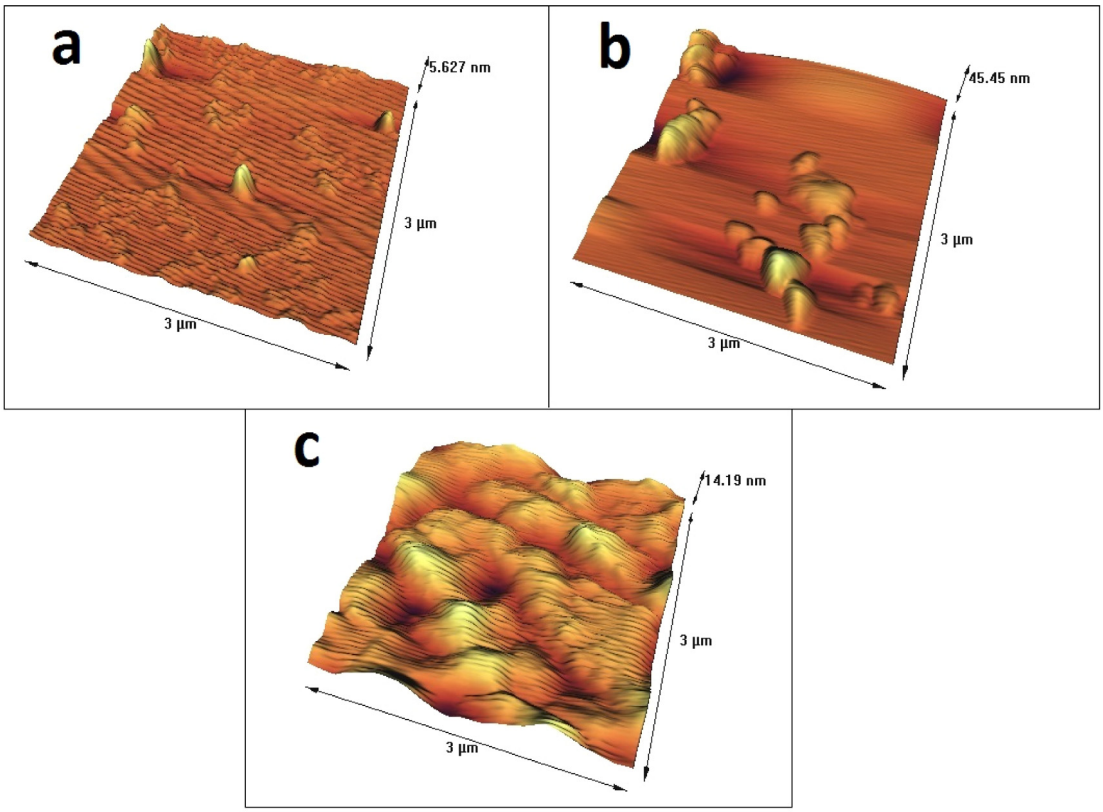

Fig. 6. 3D reconstructed images of AFM micrographs of LCNOG at different annealing temperature. (a) 650 °C (b) 750 °C (c) 850 °C.

Fig. 6a–c show a 3D images for the surface roughness which was 0.24 nm for sample at annealing temperature 640 °C up to 0.39 nm for 850 °C. From this results we found that the average particles size was equal to 78.3, 82.5 and 93.6 nm for (650, 750 and 850) °C respectively. May be the high annealing temperature caused the increase of surface roughness and of the average particle size.

When the annealing temperature increases the material gains larger energy amounts and ion diffusion increases, which leads to higher probability to form large particles and agglomerates [38–40].

Fig. 7 shows the measured hysteresis loops of LCNOG powders at different annealing temperatures (650, 750 and 850) °C and a comparison with hysteresis loops of LCNOG (target).

Magnetic permeability (μ) is fixed in the proportionality between the magnetic induction and intensity of the magnetic field. The higher magnetic permeability (μ) of the material corresponds to an increased conductivity of the magnetic lines of force, and vice versa. It refers to the ease with which the outer M can build a higher magnetic force than the attraction in matter. In general, the materials can be classified into (Diamagnetic, Paramagnetic or Ferromagnetic). Diamagnetic materials: provide opposition to external magnetic fields, Para-magnetic materials: are weakly attracted by external magnetic fields and Ferro-magnetic materials: are strongly attracted by external magnetic fields. (μ) of Ferro-magnetic materials is significantly greater than a vacuum, and as a result, they are used in building magnetic cores in magnetic circuits.

From the results, it can be observed that the LCNOG powders are paramagnetic and magnetization factor gained at 0.8 emu/g in ±15kOe external field [34,37].

The Saturation Magnetization (Ms), and Residual Magnetization (Mr) decreases with the increase in the particle size while the coercivity force (Hc) decreases with the increase in the annealing and heating temperatures.

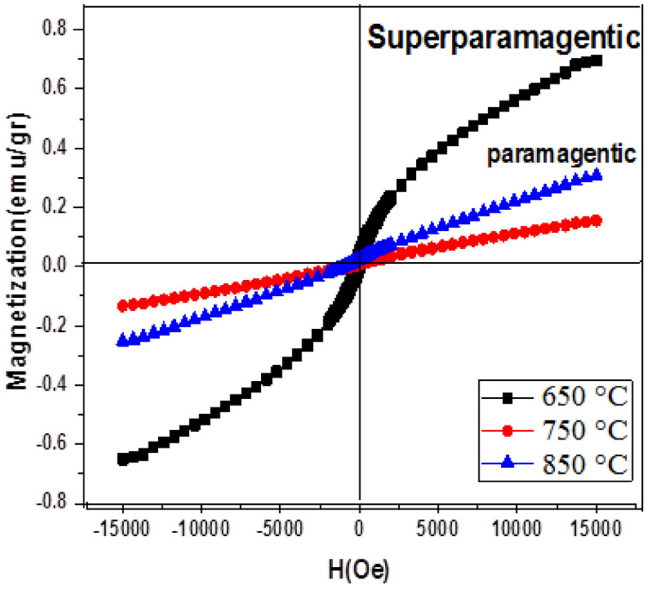

Fig. 7. Hysteresis loops of LCNOG powder annealing at (650, 750 and 850) °C and as target before annealing.

4. Conclusions

1- Magnetic measurements indicate that the improved ferromagnetic properties and improved magnetic properties are attributed to the increased Ni and Co-ferrite formation at a given combustion condition.

2- It can also be concluded that best conditions of $LiCo_{0.525}Ni_{0.475}O_2$/G (LCNOG) powder prepared by self-propagating combustion reaction for cathodes of micro-lithium ion batteries correspond to an annealing temperature of 750 °C.

References

[1] Goodenough J, Kim Y. Challenges for rechargeable Li batteries. Chem Mater 2010;22:587–603.
[2] Bruce PG, Scrosati B, Tarascon JM. Nanomaterials for rechargeable lithium batteries. Angew Chem Int Ed 2008;47:2930–46.
[3] Julien CM, Mauger A, Vijh A, Zaghib K. Lithium batteries science and technology. Springer; 2016.
[4] Tarascon JM. Key challenges in future Li-battery research. Phil Trans R Soc A 2010;368:3227–41.
[5] Patil V, Pawar S, Chougule M, Godse P, Sakhare R, Sen S, Joshi P. Effect of annealing on structural, morphological, electrical and optical studies of nickel oxide thin films. J Surf Eng Mater Adv Technol 2011;1:35–41.
[6] Grande L, Chundi VT, Wei D, Bower C, Andrew P, Ryhänen T. Graphene for energy harvesting/storage devices and printed electronics. Particuology 2012;10:1–8.
[7] Valentini L, Cardinali M, Bon SB, Bagnis D, Verdejo R, Manchado A, Kenny JM. Use of butylamine modified graphene sheets in polymer solar cells. Mater Chem 2010;20:995–1000.
[8] Qu L, Liu Y, Baek JB, Dai L. Nitrogen-doped graphene as efficient metal-free electrocatalyst for oxygen reduction in fuel cells. ACS Nano 2010;4:1321–6.
[9] Yan J, Wei T, Shao B, Fan Z, Qian W, Zhang M, Wei F. Preparation of a graphene nanosheet/polyaniline composite with high specific capacitance. Carbon 2010;48:487–93.
[10] Li Y, Wang J, Li X, Geng D, Li R, Sun X. Superior energy capacity of graphene nanosheets for a nonaqueous lithium-oxygen battery. Chem Commun 2011;47:9438–40.
[11] Lian P, Zhu X, Liang S, Li Z, Yang W, Wang H. Large reversible capacity of high quality graphene sheets as an anode material for lithium-ion batteries. Electrochim Acta 2010;55:3909–14.
[12] Sathish M, Tomai T, Honma I. Graphene anchored with Fe3O4 nanoparticles as anode for enhanced Li-ion storage. Power Sources 2012;217:85–91.
[13] https://www.azom.com/article.aspx?ArticleID=10123.
[14] Huang X, Qi X, Boey F, Zhang H. Graphene based composites. Chem Soc Rev 2012;41:666–86.
[15] Paek SM, Yoo E, Honma I. Enhanced cyclic performance and lithium storage capacity of SnO_2/graphene nanoporous electrodes with three-dimensionally delaminated flexible structure. Nano Lett 2009;9:72–5.
[16] Edwards RS, Coleman KS. Graphene synthesis: relationship to applications. Nanoscale 2013;5:38–51.

[17] Warner JH, Schaffel F, Rummeli M, Bachmatiuk A. Graphene: Fundamentals and emergent applications. Newnes; 2012.
[18] Novoselov KS, Geim AK, Morozov SV, Jiang D, Zhang Y, Dubonos SV, Grigorieva IV, Firsov AA. Electric field effect in atomically thin carbon films. Science 2004;306:666–9.
[19] Reina A, Jia X, Ho J, Nezich D, Son H, Bulovic V, Dresselhaus MS, Kong J. Large area, few-layer graphene films on arbitrary substrates by chemical vapor deposition. Nano Lett 2008;9:30–5.
[20] Dato A, Radmilovic V, Lee Z, Phillips J, Frenklach M. Substrate-free gas-phase synthesis of graphene sheets. Nano Lett 2008;8:2012–6.
[21] Verdejo R, Bernal MM, Romasanta LJ, Lopez-Manchado MA. Graphene filled polymer nanocomposites. J Mater Chem 2011;21:3301–10.
[22] Park S, Ruoff RS. Chemical methods for the production of graphenes. Nat Nanotechnol 2009;4:217–24.
[23] Bolotin KI, Sikes KJ, Jiang Z, Klima M, Fudenberg G, Hone J, Kim P, Stormer HL. Ultrahigh electron mobility in suspended graphene. Solid State Commun 2008;146:351–5.
[24] Tan KS, Reddy MV, Rao GVS, Chowdari BVR. High-performance $LiCoO_2$ by molten salt ($LiNO_3$:LiCl) synthesis for Li-ion batteries. J Power Sources 2005;147:241–8.
[25] Fu J, Bai Y, Liu C, Yu H, Mo Y. Physical characteristic study of $LiCoO_2$ prepared by molten salt synthesis method in 550–800 °C. Mater Chem Phys 2009;115:105–9.
[26] Waller GH, Lai SY, Rainwater BH, Liu M. Hydrothermal synthesis of $LiMn_2O_4$ onto carbon fiber paper current collector for binder free lithium-ion battery positive electrodes. J Power Sources 2014;251:411–6.
[27] Wang Q, Deng S, Wang H, Xie M, Liu J, Yan H. Hydrothermal synthesis of hierarchical $LiFePO_4$ microspheres for lithium ion battery. J Alloys Compd 2013;553:69–74.
[28] Jafta CJ, Ozoemena KI, Mathe MK, Roos WD. Synthesis, characterisation and electrochemical intercalation kinetics of nanostructured aluminium-doped $Li[Li_{0.2}Mn_{0.54}Ni_{0.13}Co_{0.13}]O_2$ cathode material for lithium ion battery. Electrochim Acta 2012;85:411–22.
[29] Ding YH, Zhang P, Jiang Y, Gao D. Effect of rare earth elements doping on structure and electrochemical properties of $LiNi_{1/3}Co_{1/3}Mn_{1/3}O_2$ for lithium-ion battery. Solid State Ion 2007;178:967–71.
[30] Zhu J. Synthesis, characterization and performance of cathodes for lithium ion batteries. Ph.D. University of California; 2014, p. 31–45.
[31] Haider AJ, Rsool RA, Haider MJ. Morphological and structural properties of cathode compound material for lithiumion battery. Plasmonics 2018;8:1–9.
[32] Al-Tabbakh AA, Kamarulzaman N, AL-Zubaidi AS. Synthesis and properties of a spinel cathode material for lithium ion battery with flat potential plateau. Turk J Phys 2015;39:187–98.
[33] Zhang B, Wang ZX, Guo HJ. Effect of annealing treatment on electrochemical property of $LiNi_{0.5}Mn_{1.5}O_4$ spinel. Trans Nonferrous Met Soc China 2007;17:287–90.
[34] Balasooriya NWB, Bandaranayake PWSK. Electrochemical properties of $LiCo_{0.4}Ni_{0.6}O_2$ and its performances in rechargeable lithium batteries. Sri Lankan J Phys 2007;8:47–58.
[35] Albrecht D, Wulfmeier H, Fritze H. Preparation and characterization of c-$LiMn_2O_4$ thin films prepared by PLD for lithiumion batteries. Eng Technol 2016;4:1558–64.
[36] Park M, Zhang X, Chunga M, Less GB, Sastry AM. A review of conduction phenomena in Li-ion batteries. J Power Sources 2010;195:7904–29.
[37] Philippe B, Mahmoud A, Ledeuil JB, Sougrati MT, Edström K, Dedryvère R, Gonbeau D, Lippens PE. MnSn2 electrodes for Li-ion batteries: mechanisms at the nano scale and electrode/electrolyte interface. Electrochim Acta 2014;123:72–83.
[38] Kalyani P, Kalaiselvi N. Various aspects of LiNiO2 chemistry: A review. Sci Technol Adv Mater 2005;6:689–703.
[39] Xia H, Lu L. Growth of layered $LiNi_{0.5}Mn_{0.5}O_2$ thin films by pulsed laser depositio for application in microbatteries. Appl Phys Lett 2008;92:011912–011912–3.
[40] Balakrishnan P, Veluchamy P. Synthesis and characterization of $CoFe_2O_4$ magnetic nanoparticles using sol–gel method. Int J Chem Tech Res 2015;8:271–6.